



Exploring thermal comfort of urban buildings based on local climate zones

Jiayi Ren^a, Jun Yang^{a,b,*}, Yuqing Zhang^a, Xiangming Xiao^c, Jianhong Cecilia Xia^d, Xueming Li^a, Shaohua Wang^e

^a Human Settlements Research Center, Liaoning Normal University, 116029, Dalian, China

^b Jangho Architecture College, Northeastern University, Shenyang, 110169, China

^c Department of Microbiology and Plant Biology, Center for Spatial Analysis, University of Oklahoma, Norman, OK, 73019, USA

^d School of Earth and Planetary Sciences (EPS), Curtin University, Perth, 65630, Australia

^e Key Laboratory of Digital Earth Science, Aerospace Information Research Institute, Chinese Academy of Sciences, Beijing, 100094, China

ARTICLE INFO

Handling Editor: Bin Chen

Keywords:

Local climate zone
Regional thermal environment
Thermal comfort
Energy balance
Zhengzhou City

ABSTRACT

Despite increasing attention to rising land surface temperatures (LSTs) and other climate changes caused by urbanization, few studies have considered the characteristics of LST or thermal comfort of human settlements from a regional perspective. Therefore, to explore the regional characteristics of LST and thermal comfort in Zhengzhou, China, we calculated the predicted mean vote (PMV) based on local climate zones (LCZs) using ENVI-met and studied correlations between LSTs and vegetation-type LCZs. The total land area under human settlements in Zhengzhou is 316.26 km², 52.72% of which is accounted by LCZs of buildings. The LSTs of built-up areas in this region were significantly higher than those of natural surfaces, with the highest and lowest LSTs of 37.98 °C (in LCZ3; compact low-rise buildings) and 32.46 °C (in LCZG; water areas), respectively. Under the same conditions, the PMV value was considered near “moderate” in areas with sparsely distributed buildings. LCZ7 (sparse high-rise buildings) always exhibited the lowest PMV, with an average value of −0.16 at 18:00 h. In addition, the correlations between LST and normalized difference vegetation index varied for LCZs with different types of vegetation, with the highest correlation coefficient (−0.80) observed in LCZA and the lowest correlation coefficient (−0.62) observed in LCZB. These results provide a reference for designing an optimal layout of urban facilities to regulate the thermal environment of human settlements and promoting urban sustainable development.

1. Introduction

With rapid global urban development, the natural landscape is increasingly being replaced by impervious surfaces, and concentrated human activities are changing the urban thermal environment (Panagopoulos et al., 2015; Yang et al., 2019; Yue et al., 2020; Yin et al., 2022). These conditions have led to the development of Urban Heat Islands (UHIs), which not only reduce living comfort (Kong et al., 2017; Yang et al., 2017a; Omidvar and Kim, 2020), but also profoundly influence urban ecological systems and the regional climate (Emmanuel and Krüger, 2012; Qiao et al., 2019; Portela et al., 2020). In urban thermal environments, land surface temperature (LST) is a key

parameter for determining the degree of surface warming. It is closely related to the season, time of day, impervious area, vegetation cover, water body area, population density, and other factors (Song et al., 2014; Zhou et al., 2016; Deilami et al., 2018; Liu et al., 2021; Tan et al., 2021). For example, Peng et al. (2012) analyzed LST differences in 419 major cities worldwide and highlighted the importance of vegetation in mitigating the UHI effect. By comparing the normalized cooling capacity and efficiency indices, Xue et al. (2019) found that the cooling capacity of urban wetlands was positively correlated with their areas, forms, and degrees of connectivity and was negatively correlated with the height and density of the surrounding buildings. Moreover, Yang et al. (2020a) reported that the vegetation phenology exhibited a strong negative

Abbreviations: LST, land surface temperature; LCZ, local climate zone; PMV, predicted mean vote; NTL, nighttime light; UHI, urban heat island; GDP, gross domestic product; NDVI, normalized difference vegetation index; DMSP-OLS, Defense Meteorological Satellite Program's Operational Linescan System; NPP-VIIRS, Visible Infrared Imaging Radiometer Suite of the Suomi National Polar-Orbiting Partnership.

* Corresponding author. Human Settlements Research Center, Liaoning Normal University, 116029, Dalian, China.

E-mail addresses: renjiayi_gis@163.com (J. Ren), yangjun8@mail.neu.edu.cn, yjdl204@126.com (J. Yang), zhanguyqing@lnnu.edu.cn (Y. Zhang), xiangming.xiao@ou.edu (X. Xiao), c.xia@curtin.edu.au (J.C. Xia), lixueming999@163.com (X. Li), wangshaohua@aircas.ac.cn (S. Wang).

<https://doi.org/10.1016/j.jclepro.2022.130744>

Received 28 November 2021; Received in revised form 10 January 2022; Accepted 28 January 2022

Available online 3 February 2022

0959-6526/© 2022 Elsevier Ltd. All rights reserved.

correlation with LST. Guo et al. (2020a) explored the spatial heterogeneity of LST based on multiple time-series data, revealing that urban areas exhibited an increasingly strong influence on LST. Furthermore, Zhou et al. (2018) illustrated that urbanization led to an increase in LST and suggested that the urban agglomeration effect must be considered to accurately reflect the magnitude of the UHI. However, additional research on the characteristics of LST from a regional perspective is required.

In some densely populated areas of developing countries in Asia, urban boundaries are blurring as old cities shrink and new development zones expand to accommodate social and economic development (Chen et al., 2019). Remote sensing technology supported by satellites has increased the efficiency of urban climate studies in these areas (Vahmani and Ban-Weiss, 2016). For example, Liu et al. (2017) reported that the UHI intensity exhibited significant positive correlations with the gross domestic product (GDP), population size, electricity consumption, and built-up area; the surfaces of the UHIs were larger than those of the urban built-up areas but smaller than those of urbanized areas. Nighttime light (NTL) data from the Defense Meteorological Satellite Program's Operational Linescan System (DMSP-OLS) and the Visible Infrared Imaging Radiometer Suite of the Suomi National Polar-Orbiting Partnership (NPP-VIIRS) can be used to directly obtain information on human activities and economic and social development by measuring the low-intensity light emitted by nighttime urban lights, including those from traffic flow, to reflect the urbanization level (Amaral et al., 2005; Xie and Weng, 2016). For example, You et al. (2020) analyzed spatial and temporal changes in the population in Northeast China based on NTL images and demographic statistics, providing data related to population mobility. These NTL data are advantageous in determining the extent of urban sprawl and built-up areas, and they can be applied to dynamic monitoring of the regional thermal environment (Ma et al., 2015; Hu et al., 2017; Li et al., 2020a). According to Li et al. (2019a), LST demonstrated an overall upward trend with increasing light intensity. Moreover, NTL is strongly correlated with human activities and can be an effective indicator of the distribution of the regional thermal environment (Li et al., 2020b). Therefore, in this study, we focused on the LST characteristics of human settlements obtained from NPP-VIIRS NTL data instead of data extracted from administrative divisions.

In addition to the blurring of boundaries between cities and built-up areas, the complexity of internal structures of human settlements (Oke, 1973) should be considered in climate improvement and energy cycle research. To comprehensively consider the influence of three-dimensional (3D) urban forms, Stewart and Oke (2012) divided the urban climate into 17 LCZs each with different combinations of buildings, land covers, vegetation, and other ground objects. The LCZs have been widely used to analyze the spatiotemporal characteristics of LST using remote sensing data (Bartessaghi Koc et al., 2018; Budhiraja et al., 2019; Hu et al., 2019). The surface properties of LCZs, such as reflectivity, water permeability, vegetation coverage, and patch size, affect LST (Yu et al., 2019; Hofierka et al., 2020; Yang et al., 2020b). In addition, building concentration affects urban ventilation and heat dissipation in both the vertical and horizontal directions, leading to heat accumulation (Steenveld et al., 2018; Ao et al., 2019; Feng et al., 2019; Yang et al., 2019a; Xie et al., 2020). Using ENVI-met software, the numerical distributions of the ground temperature can be calculated with high accuracy using building models utilizing meteorological parameters; therefore, the software is widely used in outdoor microclimate environment simulations (Bande et al., 2020; Berardi et al., 2020; Sundus and Bassam, 2020). Most previous studies identifying urban and rural fringe areas featured statistical analysis methods, comprehensively considering single- or multi-factor indicators, such as population density, proportion of built-up land, proportion of non-agricultural population, and economic level (Ren et al., 2011; Lenzholzer, 2012; Yang et al., 2017b; He, 2018). The LCZ system resolves mismatches between landscape descriptions and regional climate classifications (Peng et al., 2018; Yang et al., 2021a, 2021b), and NTL data are not restricted by

administrative region (Zhao, 2018). Thus, we used NTL data to extract the boundaries of human settlement environment by data comparison and studied the characteristics of the urban thermal environment based on LCZs.

The ENVI-met software is suitable for simulating the urban microclimate environments of small- and medium-sized urban blocks, building roofs, and green spaces. It comprehensively considers factors such as wind speed, temperature, human metabolism, and water vapor exchange between skin and air on the human surface and has been employed in several previous studies (Milesi et al., 2003; Guo et al., 2019; Li et al., 2019b; Ouyang et al., 2020; Yang et al., 2021c). When building LCZ models, different materials are assigned to the surface to resemble the actual conditions. Moreover, a more accurate numerical distribution can be obtained using calculations based on meteorological data (Bruse and Fleer, 1998). However, a modeling method based on a 3D rectangular network with a maximum limited mesh number of $250 \times 250 \times 30$ may result in inaccuracies compared with the actual conditions (Simona et al., 2018). Existing studies have predominantly focused on small-scale blocks or single buildings. In contrast, this study incorporated nine LCZ categories for built-up areas in the model using ENVI-met software, facilitating the acquisition of residential thermal comfort levels for different LCZs.

In this study, we used multisource data to simulate thermal comfort in the municipal district of Zhengzhou using the LCZ system. From a view of emphasizing on regional complexity, the aims of this study were to (1) identify LST features of human settlements using a Geographic Information System (GIS) spatial analysis method based on Landsat-8, NTL, and meteorological data, and (2) construct models to simulate and calculate human thermal comfort in different LCZs using ENVI-met software. The results provide useful references for designing urban infrastructure and layouts, regulating urban thermal environments, and improving the quality of life of area residents.

2. Research data and methods

2.1. Study area

Zhengzhou ($34^{\circ}16' - 34^{\circ}58' \text{ N}$, $112^{\circ}42' - 114^{\circ}14' \text{ E}$) is in central China. The terrain altitude of this region is high in the southwest and low in the northeast, and the region exhibits a temperate continental monsoon climate with four distinct seasons. The annual average temperature is 15.6°C . August is the hottest month of the year, with a monthly average temperature of 25.9°C , whereas January is the coldest month, with a monthly average temperature of 2.15°C . A city rich in natural resources, Zhengzhou is a vital hub for railway transport, aviation, and electric power. In 2019, the urban population was 7.721 million and the city had an urbanization rate of 74.6% (USFD, 2019). Therefore, the municipal district of Zhengzhou (Fig. 1) was selected as the study area to provide a reference for rational urban construction.

2.2. Research data

The research data employed in this study included remote sensing images, meteorological data, and building distribution, as presented in Table 1. The original NPP-VIIRS data type was floating-point; light not produced by human populations, such as stray light, lightning, and lunar illumination were filtered out of the dataset. These images were also de-noised for more uniform brightness. Because the focus of this study was on the thermal comfort of LCZs at a specific time, we selected Landsat-8 images with sunny days and low cloud cover on July 7. We then processed them using the ENVI5.3 FLAASH atmospheric correction module to eliminate water vapor and other effects before use. The building data for Zhengzhou included building height (BH) and number of floors. The computational geometry tool in ArcGIS 10.2 was used to obtain the base area of the building. Building types were classified according to the current national General Rules for Civil Building Design (GB50352-

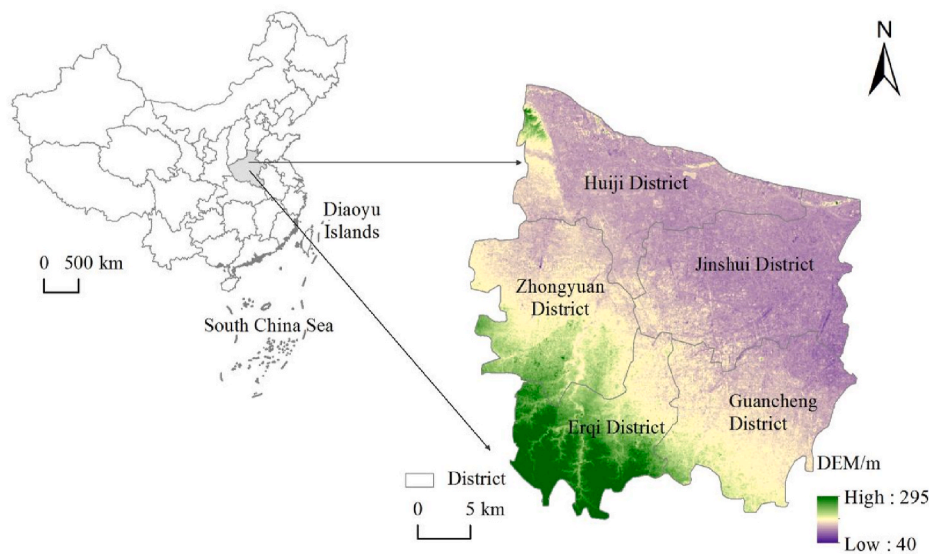
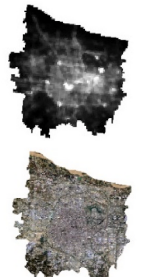



Fig. 1. Overview of the study area.

Table 1
Data sources and interpretation.

Types	Description	Sources	Sample
Remote Sensing data	NPP-VIIRS Resolution: 500 m; Day: 2019-7	earthexplorer.usgs.gov	
	Landsat8 OLI-TIRS LC81240362019188LGN00; Date: 2019-7-7; Cloud cover<5%		
Building data	Building outline contains height and floor information	Baidumap	
Meteorological data	Meteorological site data air temperature, pressure, relative humidity	rp5.ru	—

2019), and Landsat-8 images were used as supporting data for LCZ mapping. Finally, meteorological data were employed to determine the weather conditions and LST inversion.

2.3. Methods

2.3.1. LCZ mapping and human settlement environments

In the LCZ system of Stewart and Oke (2012), building cover is described by BH and building density (BD). Land cover is categorized with the following types: high-density vegetation area, low-density vegetation area, shrub area, low vegetation area, hard ground (bare rock or paved ground), sandy land (bare soil or sand), and water body. In this study, ENVI5.3 was used to classify the land cover types by the random forest classification method (Huang et al., 2016). Because of the large computational load, training samples were initially collected, and a decision tree was later derived in the experimental area to obtain the LCZ land cover categories, such as LCZA–G. The Create Fishnet tool was used to calculate the lattice network BD and average BH (Wang et al., 2017) for 30 × 30 m units (Fig. 2), which were used to classify the LCZ buildings, the categories LCZ1–9. Regarding the Zhengzhou City

residential building structure, the industrial zone is typically distributed outside the city as large low-rise buildings; therefore, LCZ10 was classified as factories (heavy industry). The BD and BH were calculated as follows:

$$BD = \frac{\sum_i A_i}{S} \tag{1}$$

$$BH = \frac{\sum_i (A_i N_i) \Delta H}{\sum_i A_i} \tag{2}$$

where A_i , N_i , and ΔH denote the floor area of the building, number of floors, and average height (typically 3 m), respectively, and S denotes the total land area, (the area per unit grid). The buildings were divided according to their density into compact, open, and sparse categories. In addition, the buildings were classified as low-rise, mid-rise, or high-rise buildings if their heights were <10 m, 10–27 m, or >27 m, respectively. Finally, the study area was divided into 17 LCZs (Table 2).

ArcGIS 10.2 was used to calculate the light spot areas of the NTL images, and the threshold method was used to extract the human settlement environments in combination with the Notice on the Size of

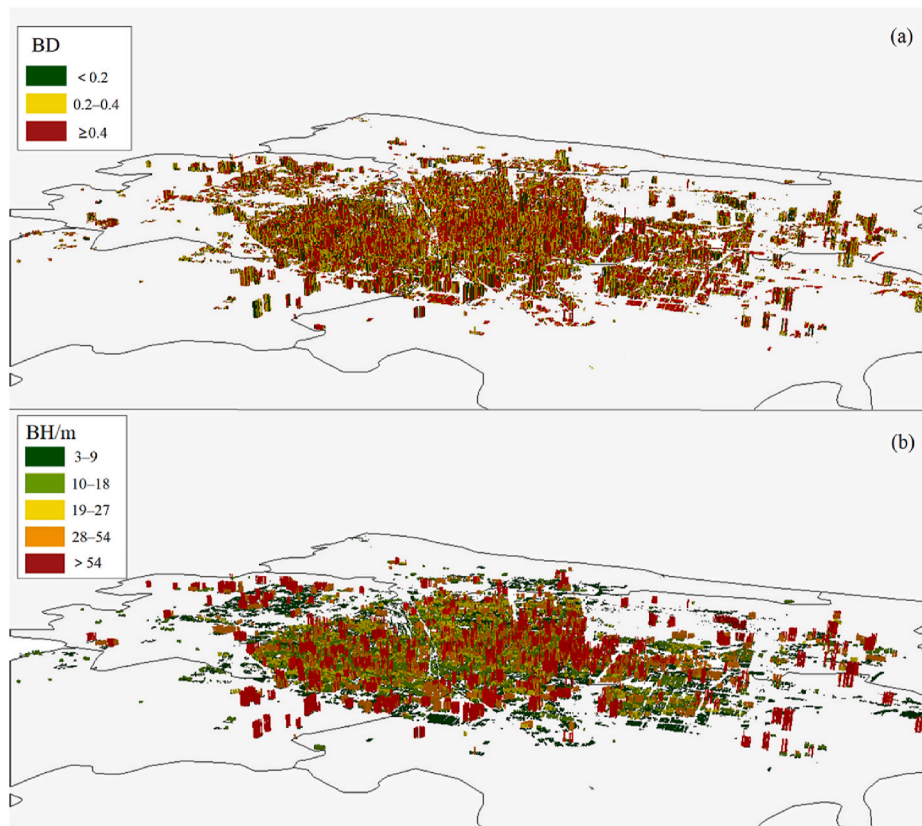


Fig. 2. Spatial distribution of buildings in Zhengzhou.

Table 2
LCZ classification types (Stewart et al., 2014).

Building LCZs	Explanation	Nature LCZs	Explanation
LCZ1	Compact high-rise	LCZA	Dense trees
LCZ2	Compact mid-rise	LCZB	Scattered trees
LCZ3	Compact low-rise	LCZC	Bush, scrub
LCZ4	Open high-rise	LCZD	Low plants
LCZ5	Open mid-rise	LCZE	Bare rock or paved
LCZ6	Open low-rise	LCZF	Bare soil or sand
LCZ7	Sparse high-rise	LCZG	Water area
LCZ8	Sparse mid-rise		
LCZ9	Sparse low-rise		
LCZ10	Heavy industry		

Zhengzhou Urban Built-up Area, published by the Zhengzhou Municipal Government in 2019 (Table 3) (Li et al., 2007; Shi et al., 2014).

This study adopted the data comparison method to conduct segmented statistics on the NPP-VIIRS data (Table 4) and extract the boundary of human settlement environments. The digital number (DN) range for Zhengzhou was 62–188, and the pixel areas with DN values greater than 150 and 160 were 433.26 km² and 295.61 km², respectively. In 2019, the built-up area was 319.28 km²; therefore, the gray threshold was between 150 and 160. Thus, the DN threshold value was determined as 159, corresponding to a living environment area of 316.26 km².

Table 3
Built-up area of the central city.

District	Jinshui	Erqi	Guancheng	Zhongyuan	Huiji	Sum
Administrative area/km ²	242.34	156.22	199.61	198.14	222.50	1018.81
Built-up area/km ²	79.96	63.78	61.59	58.54	55.41	319.28

Table 4
NTL brightness range and pixel areas in Zhengzhou.

DN value	Number	Area/km ²	DN value	Number	Area/km ²
≤100	70	116.40	140–150	70	120.81
100–110	39	66.07	150–160	79	137.65
110–120	37	61.98	160–170	87	170.06
120–130	64	106.48	170–180	56	98.53
130–140	69	112.28	180–188	13	27.02

2.3.2. LST inversion algorithm

The study period exhibited low precipitation and sunny weather, resulting in a more significant UHI effect. The remote sensing images obtained were clear enough for inversion. In this study, we estimated LST by combining the single-window algorithm (Qin et al., 2001) with the TM10 band of the Landsat-8 images (Hu et al., 2015) according to the following formulas:

$$T_s = (a(1 - C - D) + (b(1 - C - D) + C + D)T_{10} - DT_a)/(C - 237.15), \quad (3)$$

$$C = \varepsilon\tau \quad (4)$$

$$D = (1 - \tau)[1 + (1 - \varepsilon)\tau], \quad (5)$$

where T_s , T_{10} , and T_a respectively represent the surface temperature (K), brightness temperature on the sensor (K), and average atmospheric temperature (K); a and b are the reference coefficients (when LST is in the range of 0–70 °C, $a = -67.355351$ and $b = 0.458606$); ε represents

the surface emissivity of T_{10} ; and τ represents the atmospheric transmittance of T_{10} . Finally, the surface temperature was converted from the thermodynamic temperature unit (K) to Celsius ($^{\circ}\text{C}$).

2.3.3. Comfort simulation and calculation

The Spaces plug-in in ENVI-met ($30 \times 30 \times 30 \text{ m}$) was employed to construct the LCZ models. The building LCZ models were loaded into the Guide plug-in, and the meteorological parameters were set. Among the parameters, the wind speed was 3.9 m/s, wind direction was 45° , and minimum and maximum air temperature was 22°C and 31°C and minimum and maximum relative humidity was 31% and 83%, respectively. The plug-ins were run in ENVI-core to simulate the thermal environment of human habitation. The BioMet module was used to calculate a comprehensive thermal environment evaluation index based on the PMV which considers environmental factors to evaluate the thermal comfort of the human body. A PMV value near 0 (neutral) indicates that the human body feels the most comfortable, while PMV values of 1 (−1), 2 (−2), and 3 (−3) represent feelings of being slightly warm (slightly cool), warm (cool), and hot (cold), respectively.

2.3.4. Statistical analysis

The data were statistically analyzed after the numerical simulation to compare the simulation results of each period to obtain the thermal comfort index for each LCZ type. In addition, vegetation has a cooling effect, but the specific correlation of between vegetation and natural LCZs has not been extensively studied. Therefore, we calculated the

normalized difference vegetation index (NDVI) using Band Math tool in ENVI5.3 and discussed the correlation between NDVI and LST based on LCZ. The correlation coefficient (r) between LST and NDVI was calculated using SPSS 24.0 software after excluding outliers. The formula was as follows:

$$r = \frac{\sum (x - \bar{x})(y - \bar{y})}{\sqrt{\sum (x - \bar{x})^2 \sum (y - \bar{y})^2}} \quad (6)$$

where x and y represent the observed values of the variables, while \bar{x} and \bar{y} represent the mean values of the variables.

3. Results

3.1. LCZ spatial pattern

After image processing, grayscale differentiation of the NTL images was used to improve the reflected range of human activities. By comparing the total built-up area (319.28 km^2) with the spot area of the NTL data, areas with DN values higher than 159 were extracted as human settlement areas. Thus, the total area of human settlements in the study area was 316.26 km^2 . The areas of human settlements in the Jinshui, Huiji, Zhongyuan, Erqi, and Guancheng areas were 134.82 km^2 , 15.38 km^2 , 58.22 km^2 , 35.04 km^2 , and 72.80 km^2 , respectively, which accounted for 55.63%, 6.91%, 29.38%, 22.43%, and 36.47% of the area of each district, respectively. The spatial pattern of the LCZs is

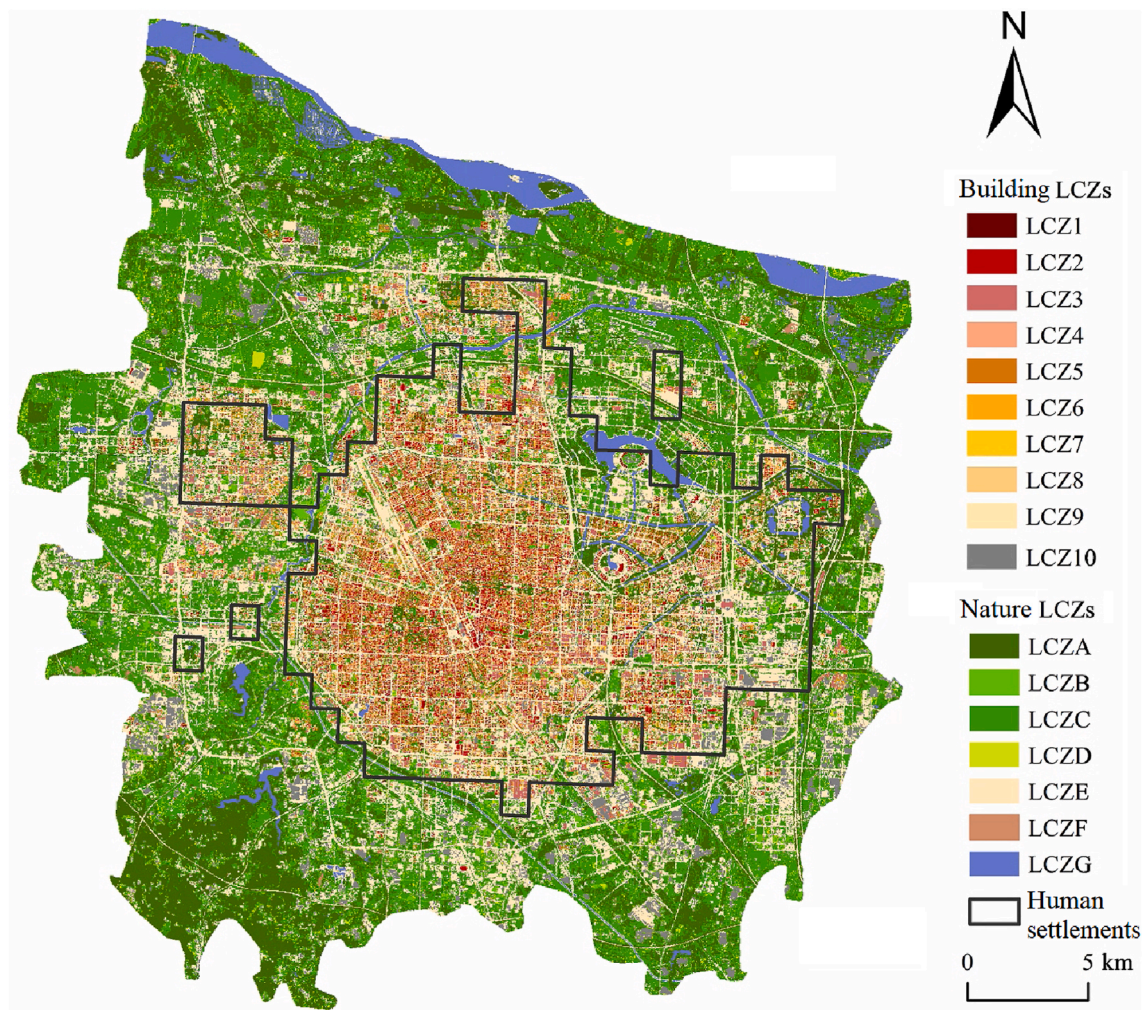


Fig. 3. LCZ mapping results and distribution of human settlements.

demonstrated in Fig. 3. The buildings in the city center were densely distributed and predominantly fell into the categories of LCZ1, LCZ2, and LCZ4. LCZ10 buildings were typically distributed in the periphery of the urban area, and urban parks were primarily LCZB and LCZG. Each type of LCZ was observed in the study area. The zones LCZ1–10, LCZA, LCZB, LCZC, LCZD, LCZE, LCZF, and LCZG accounted for 52.72%, 11.08%, 3.64%, 18.74%, 1.69%, 5.70%, 1.17%, and 5.26% of the total inhabited area, respectively.

3.2. Urban thermal environment

The LST values obtained from the Landsat-8 image inversions are presented in Fig. 4. The spatial distribution demonstrated that the LSTs of the building areas (LCZ1–10) were higher than those of green spaces and water bodies in the city. The city center and some factories exhibited the highest temperatures, while the northern rivers and city parks had the lowest temperatures. The average LSTs in the districts of Zhengzhou decreased in the following order: Zhongyuan > Guancheng > Jinshui > Erqi > Huiji (Table 5). The highest and lowest LST values among LCZA–G were in LCZB (37.53 °C) and LCZG (32.46 °C), respectively. The highest and lowest LST values among LCZ1–10 were in LCZ3 (37.98 °C) and LCZ4 (35.99 °C), respectively (Fig. 5). The LST values of the LCZ building category were significantly higher than those of the natural land cover categories. Regarding the horizontal spatial distribution, compact buildings exhibited higher LST values. Considering the vertical spatial distribution among the compact buildings (LCZ1–3), the highest LST (37.98 °C) was observed in LCZ3, (low-rise buildings), and the lowest LST (36.22 °C) was observed in LCZ1 (high-rise buildings). Among LCZ4–6 (open buildings), the highest LST value (37.36 °C) was observed in LCZ5 (mid-rise buildings), and the lowest LST (35.99 °C) was observed in LCZ4 (high-rise buildings). Among LCZ7–9 (sparse buildings), the LST values were lower for LCZ7 (high-rise buildings; 36.78 °C) than for LCZ8 (mid-rise buildings; 37.16 °C) and LCZ9 (low-rise buildings; 37.10 °C). In addition, the average LST of LCZ10 (industrial buildings) was similar to that of LCZ5 and LCZ6.

Table 5

LST numerical statistics.

District	LST _{min} /°C	LST _{max} /°C	LST _{mean} /°C
Jinshui	25.02	51.28	36.36
Erqi	27.86	52.43	36.07
Guancheng	21.09	54.11	37.33
Zhongyuan	27.42	50.83	37.78
Huiji	25.06	47.44	35.28

3.3. LCZ thermal comfort

In this study, thermal comfort was simulated for LCZ1–9, the zones that encompassed the majority of the population in the study area. Measurements for analysis were recorded three times in a day and were characterized by large outdoor human flows (Table 6); the dark blue to red colors in Table 6 indicate the changes in the PMV values from low to high. Under the same conditions, different building layouts exhibited different levels of thermal comfort. The airflow velocity decreased in the built-up areas, which was not conducive to heat diffusion and led to high PMV values. The PMV values were near zero when buildings were more sparsely distributed. In addition, some of the solar radiation was blocked by the surrounding opaque buildings and did not reach the ground in the internal space of the building groups. Therefore, the LSTs on the shadow sides of tall buildings were lower than those on the sunlit sides, thereby increasing the thermal comfort. As illustrated in Fig. 6, the PMV values varied at different times within the same LCZ; however, the overall change was negligible. At 10:00 h, the thermal comfort levels ranged from slightly warm to warm. At 14:00 h and 18:00 h, the thermal comfort levels were predominantly neutral to slightly warm. Furthermore, the PMV value declined with a decrease in the BH. The lowest PMV was consistently in LCZ7, between neutral and slightly cool, because the high-rise buildings blocked some of the incoming solar radiation. Low-density building layouts also lead to a lower LST because they can dissipate heat over time. Therefore, during urban construction, controlling the BD or increasing the BH can improve the regional

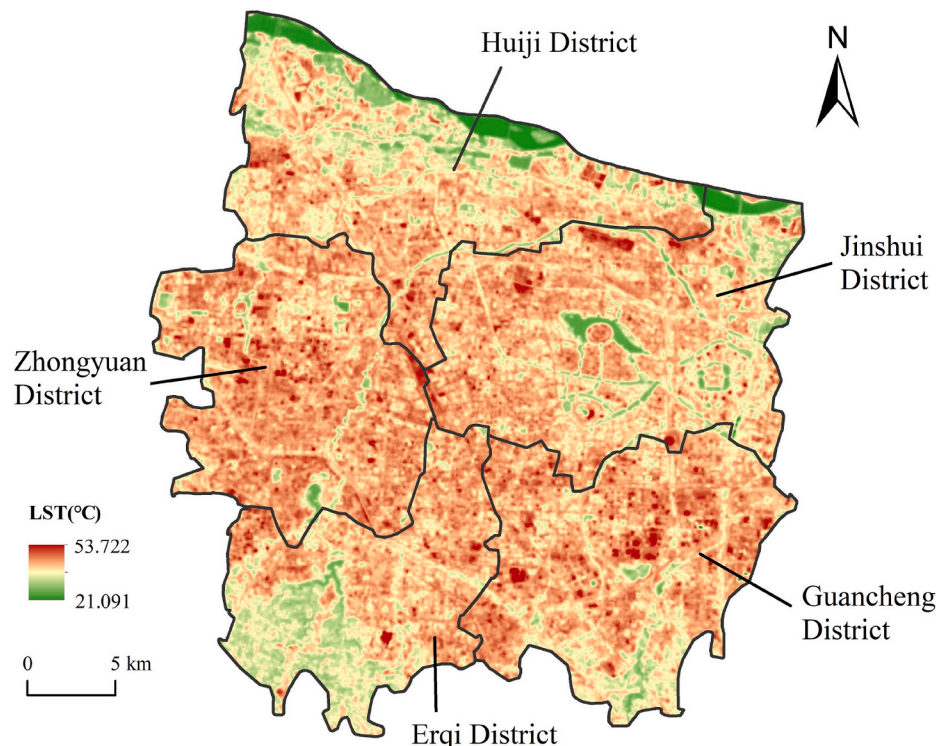


Fig. 4. Spatial distribution of LST.

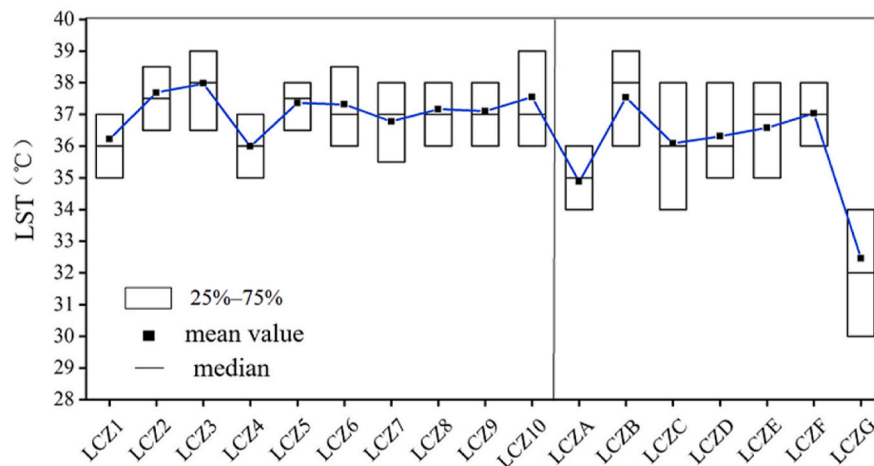


Fig. 5. Box plots with LSTs within each LCZ.

thermal environment and increase the thermal comfort of residents.

4. Discussion

4.1. Determining human settlement environments

The NPP-VIIRS data employed in this study exhibited a higher resolution than that of the DMSP-OLS remote sensing data (Shen et al., 2019). The NPP-VIIRS brightness values are influenced by architectural, climatic, and social factors (e.g., GDP). Therefore, they reflect urban characteristics and expansion trends (Levin and Zhang, 2017; Shen et al., 2019). When using NTL data to extract built-up areas, the boundary range is delimited by selecting the point of an abrupt intensity change (Zhou et al., 2015) or using the town range of the TM/ETM + data as a reference for the nightlight image and adjusting the threshold for demarcation (Imhoff et al., 1997). Because of insufficient universal mutation detection and empirical threshold methods, this study employed a data comparison method to extract the boundary of human settlement environments.

4.2. Factors influencing the thermal environment of human settlements

A change in the urban thermal environment can profoundly affect the comfort of human habitation (Qiao et al., 2013; Wang et al., 2016). Peng et al. (2016) found that built-up areas and bare land exhibited significant detrimental impacts on the thermal environment, whereas ecological land mitigated the impact of UHIs. Yang et al. (2019b) analyzed the influence of building forms on the LST under different wind conditions and demonstrated that the urban building pattern is a critical driving factor of climate change, with compact high-rise buildings increasing the LST, particularly in LCZ4, LCZ7, and LCZ8. Guo et al. (2020b) explored the driving factors of the LST at the community scale and found the LST was more influenced by spatial variables (e.g., land use) than the building form. This study found that although the LSTs of building LCZs were significantly higher than those of natural land cover LCZs, the LSTs of compact low-rise buildings were higher than those of high-rise buildings with an open or sparse layout (Xie et al., 2022). Additionally, identifying cooling factors could help improve urban ecology (Yue and Xu, 2013; He et al., 2019; Ke et al., 2021), and vegetation has different effects on LST depending on the LSZ (Luo et al., 2021). We used the NDVI to reflect the vegetation coverage, focusing on the correlation between the vegetation coverage and LST for various LCZs. There was a significant negative correlation between the NDVI and LST, and the correlations were different among LCZA–D. Fig. 7 shows a scatter plot with excluded and randomly sampled outliers. The correlation was the strongest in LCZA ($r = -0.80$), followed by LCZD

and LCZC ($r = -0.79$ and -0.74 , respectively), and the minimum correlation was in LCZB (-0.62).

4.3. Limitations

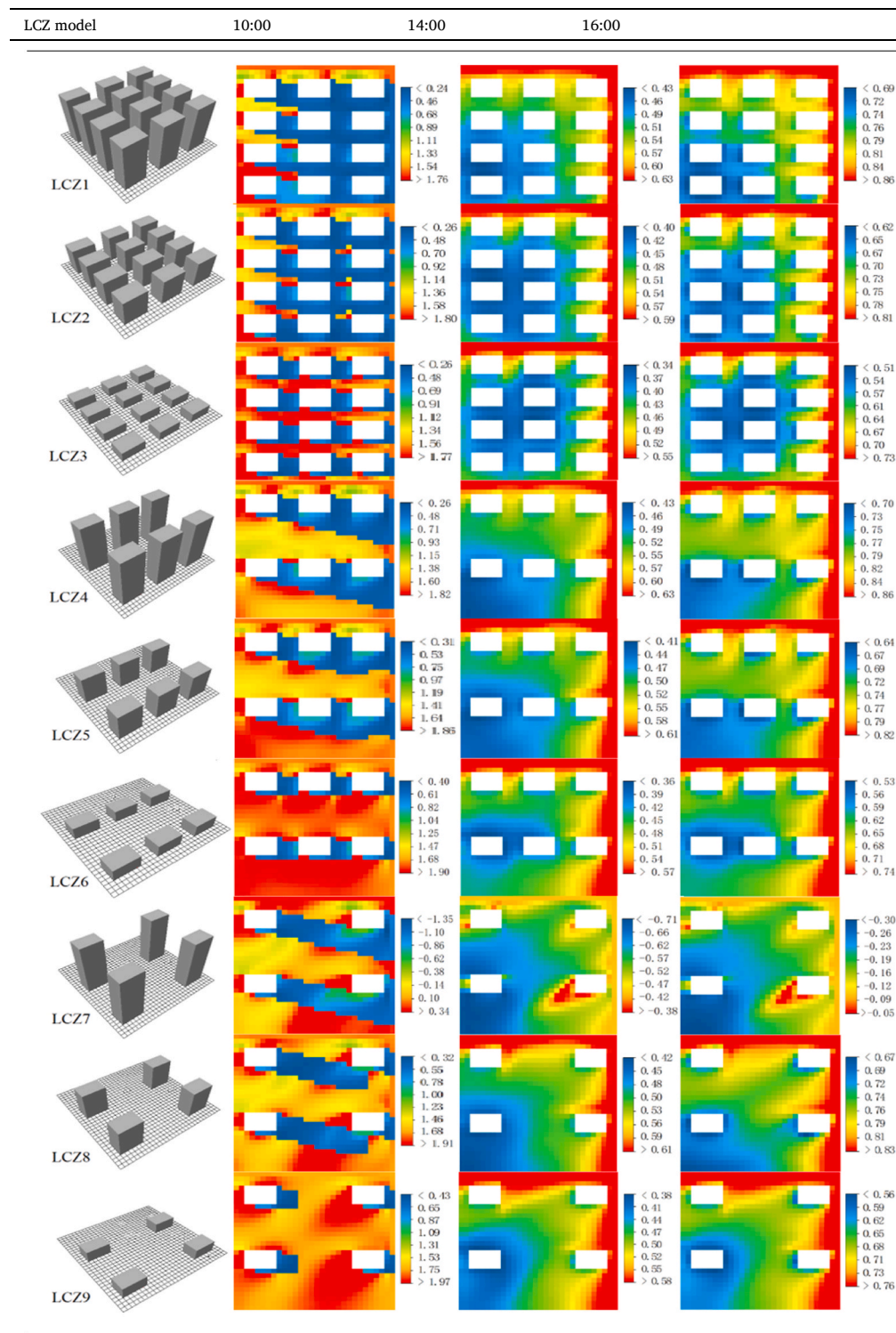
This study focused on the distribution of thermal environment under different LCZ combinations from the regional perspective and reflected the impacts of varying thermal environmental conditions on the human body using the thermal comfort index, primarily considering buildings and vegetation. However, the influencing factors of thermal environment are comprehensive and include surface water, anthropogenic heat, and various meteorological conditions. Thus, future research should include these factors.

5. Conclusions

Changes in urban LSTs have a direct impact on human comfort levels (Kleerekoper et al., 2012; Zheng et al., 2020). In this study, we applied the GIS spatial analysis method, combined with Landsat-8, NTL, and meteorological data, to explore the LST characteristics of human settlement environments in Zhengzhou. Furthermore, the urban thermal environment in different LCZs was simulated using ENVI-met software, PMV thermal comfort index was calculated for each LCZ, and the correlation between vegetation-type LCZs and LST was analyzed. The following major conclusions were formed:

- (1) The total residential area of Zhengzhou is 316.26 km², and all LCZ types were distributed in human settlements in the study area. Among the different LCZs identified in Zhengzhou, LCZ1–10 (building LCZs) accounted for the highest proportion (52.72%), while LCZF accounted for the lowest proportion (1.17%).
- (2) LST of the building LCZs was significantly higher than that of the natural land cover LCZs, with the highest LST (37.98 °C) observed in compact low-rise buildings (LCZ3) and the lowest LST (32.46 °C) observed in water areas (LCZG). Generally, the more compact the building distribution, the higher the LST. However, high-rise buildings blocked solar radiation and reduced the LST for the LCZs in their shadows.
- (3) For building LCZs under the same conditions, thermal comfort levels were predominantly slightly warm to warm at 10:00 h, but they were typically neutral and slightly warm at 14:00 h and 18:00 h. The PMV value was consistently low for sparsely distributed high-rise buildings (LCZ7), with an average value of -0.16 at 18:00 h, which was the closest to neutral thermal comfort. In addition, the correlation between LST and NDVI was

Table 6
Simulation results of thermal comfort in LCZ1–9.



different among LCZA–D, with the highest correlation coefficient being -0.80 (LCZA) and the lowest being -0.62 (LCZB).

Therefore, increasing the green area and optimizing the layout of buildings by accounting for the height and density of buildings to improve the local climate and increase the comfort of residents should be considered in urban construction.

CRediT authorship contribution statement

Jiayi Ren: Data curation, Software, Writing – review & editing. **Jun Yang:** Conceptualization, Methodology, Software. **Yuqing Zhang:** Writing – review & editing, Methodology, Software. **Xiangming Xiao:** Writing – review & editing. **Jianhong Cecilia Xia:** Writing – review & editing. **Xueming Li:** Data curation, Writing – review & editing. **Shaohua Wang:** Data curation, Writing – review & editing.

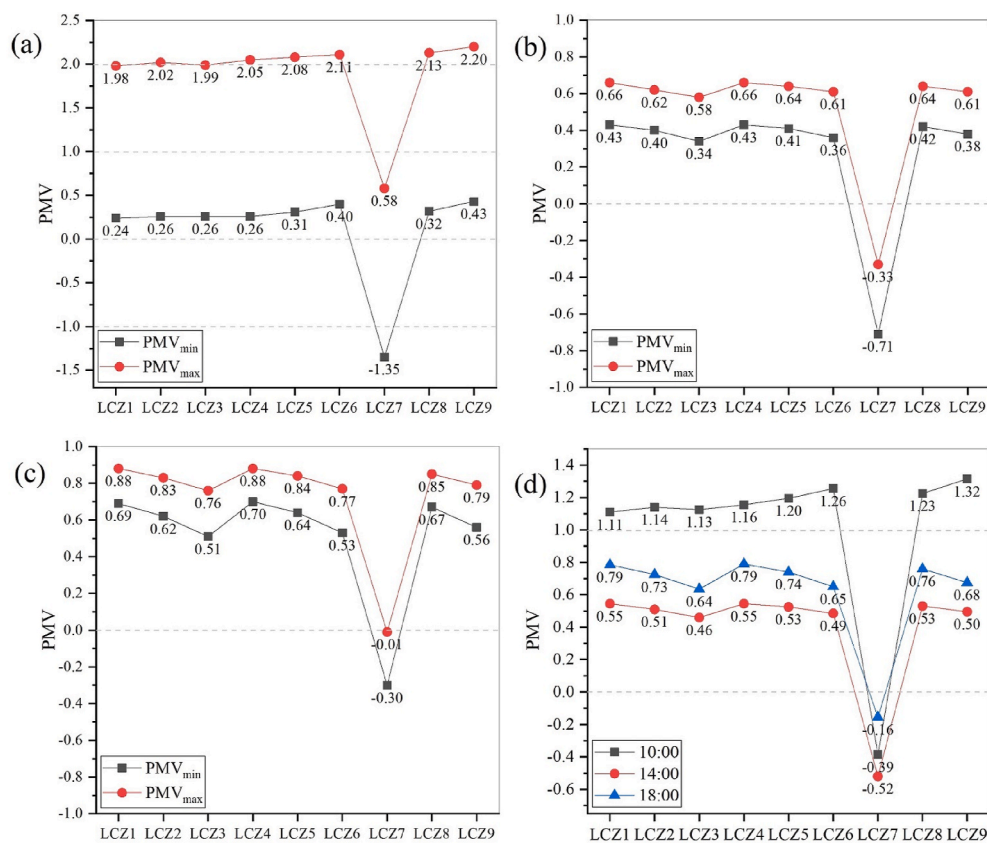


Fig. 6. Line diagram of PMV change in LCZ1-9 at 10:00 h (a), 14:00 h (b), 18:00 h (c), and mean of PMV (d).

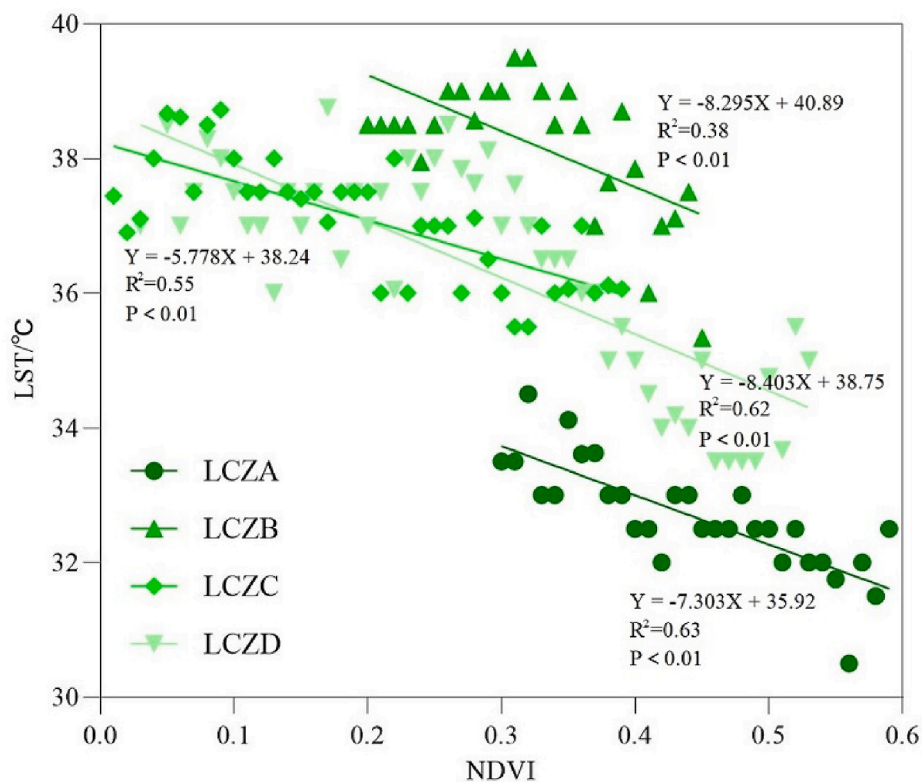


Fig. 7. LST and NDVI scatter plots in LCZA-D.

Declaration of competing interest

The authors declare that they have no known competing financial interests or personal relationships that could have appeared to influence the work reported in this paper.

Acknowledgments

This research study was supported by the National Natural Science Foundation of China (grant no. 41771178, 42030409, 41671151), the Fundamental Research Funds for the Central Universities (grant no. N2111003), Basic Scientific Research Project (Key Project) of the Education Department of Liaoning Province (grant no. LJKZ0964), Natural Science Foundation of Guizhou Province (grant no. [2019]1150), the Second Tibetan Plateau Scientific Expedition and Research Program (STEP) (grant no. 2019QZKK1004), and Innovative Talents Support Program of Liaoning Province (Grant No. LR2017017).

References

- Amaral, S., Câmara, G., et al., 2005. Estimating population and energy consumption in Brazilian Amazonia using DMSP night-time satellite data. *Comput. Environ. Urban Syst.* 29 (2), 179–195.
- Ao, X.Y., Tan, J.G., Zhi, X., et al., 2019. Synergistic interaction between urban heat island and heat waves and its impact factors in Shanghai. *Acta Geograph. Sin.* 74 (9), 1789–1802.
- Bande, L., Manandhar, P., Ghazal, R., et al., 2020. Characterization of local climate zones using ENVI-met and site data in the city of Al-Ain, UAE. *Int. J. Sustain. Dev. Plann.* 15 (5), 751–760.
- Bartasaghi Koc, C., Osmond, P., Peters, A., et al., 2018. Understanding land surface temperature differences of local climate zones based on airborne remote sensing data. *IEEE J. Sel. Top. Appl. Earth Obs. Rem. Sens.* 11 (8), 2724–2730.
- Berardi, U., Jandaghian, Z., Graham, J., 2020. Effects of greenery enhancements for the resilience to heat waves: a comparison of analysis performed through mesoscale (WRF) and microscale (Envi-met) modeling. *Sci. Total Environ.* 747, 141300. <https://doi.org/10.1016/j.scitotenv.2020.141300>.
- Budhiraja, B., Gawuc, L., Agrawal, G., 2019. Seasonality of surface urban heat island in Delhi city region measured by local climate zones and conventional indicators. *IEEE J. Sel. Top. Appl. Earth Obs. Rem. Sens.* 12 (12), 5223–5232.
- Bruse, M., Fleer, H., 1998. Simulating surface-plant-air interactions inside urban environments with a three dimensional numerical model. *Environ. Model. Software* 13, 373–384.
- Chen, Z.Q., Yu, B.L., Zhou, Y.Y., et al., 2019. Mapping global urban areas from 2000 to 2012 using time-series nighttime light data and MODIS products. *IEEE J. Sel. Top. Appl. Earth Obs. Rem. Sens.* 12 (4), 1143–1153.
- Deilami, K., Kamruzzaman, M., Liu, Y., 2018. Urban heat island effect: a systematic review of spatio-temporal factors, data, methods, and mitigation measures. *Int. J. Appl. Earth Obs. Geoinf.* 67, 30–42.
- Emmanuel, R., Krüger, E., 2012. Urban Heat Island and its Impact on Climate Change Resilience in a Shrinking City: the Case of Glasgow, UK, vol. 53. Building and Environment, pp. 137–149.
- Feng, Z.X., Wang, S.J., Jin, S.H., Yang, J., 2019. Effects of urban morphology and wind conditions on land surface temperature in Changchun. *Acta Geograph. Sin.* 74 (5), 902–911.
- Guo, A.D., Yang, J., Sun, W., et al., 2020a. Impact of urban morphology and landscape characteristics on spatiotemporal heterogeneity of land surface temperature. *Sustain. Cities Soc.* <https://doi.org/10.1016/j.scs.2020.102443>.
- Guo, A.D., Yang, J., Xiao, X.M., et al., 2020b. Influences of urban spatial form on urban heat island effects at the community level in China. *Sustain. Cities Soc.* 53, 1–12.
- Guo, C., Buccolieri, R., Gao, Z., 2019. Characterizing the morphology of real street models and modeling its effect on thermal environment. *Energy Build.* 203, 109433.
- He, B.J., 2018. Potentials of meteorological characteristics and synoptic conditions to mitigate urban heat island effects. *Urban Clim.* 24, 26–33. <https://doi.org/10.1016/j.uclim.2018.01.004>.
- He, B.J., Ding, L., Prasad, D., 2019. Enhancing urban ventilation performance through the development of precinct ventilation zones: a case study based on the Greater Sydney, Australia. *Sustain. Cities Soc.* 47, 101472 <https://doi.org/10.1016/j.scs.2019.101472>.
- Hofierka, J., Gallay, M., Onacillová, K., et al., 2020. Physically-based land surface temperature modeling in urban areas using a 3-D city model and multispectral satellite data. *Urban Clim.* 31, 100566 <https://doi.org/10.1016/j.uclim.2019.100566>.
- Hu, D.Y., Qiao, K., Wang, X.L., 2015. Land surface temperature retrieval from Landsat 8 thermal infrared data using mono-window algorithm. *J. Rem. Sens.* 19 (6), 964–976.
- Hu, J., Yang, Y.B., Pan, X., et al., 2019. Analysis of the spatial and temporal variations of land surface temperature based on local climate zones: a case study in Nanjing, China. *IEEE J. Sel. Top. Appl. Earth Obs. Rem. Sens.* 12 (11), 4213–4223.
- Hu, Y.N., Peng, J., Liu, Y.X., et al., 2017. Mapping development pattern in Beijing-Tianjin-Hebei urban agglomeration using DMSP/OLS nighttime light data. *Rem. Sens.* 9 (7).
- Huang, X., Schneider, A., Mark, A.M., et al., 2016. Mapping sub-pixel urban expansion in China using MODIS and DMSP/OLS nighttime lights. *Rem. Sens. Environ.* (175), 92–108.
- Imhoff, M.L., Lawrence, W.T., Elvidge, C.D., et al., 1997. Using nighttime DMSP/OLS images of city lights to estimate the impact of urban land use on soil resources in the United States. *Rem. Sens. Environ.* 59 (1), 105–117.
- Ke, X.L., Men, H.L., Zhou, T., et al., 2021. Variance of the impact of urban green space on the urban heat island effect among different urban functional zones: a case study in Wuhan. *Urban For. Urban Green.* <https://doi.org/10.1016/J.UFUG.2021.127159>.
- Kleerekoper, L., Esch, M., Salcedo, T.B., 2012. How to make a city climate-proof, addressing the urban heat island effect. *Resour. Conserv. Recycl.* 64, 30–38.
- Kong, L., Lau, K.K., Yuan, C., et al., 2017. Regulation of outdoor thermal comfort by trees in Hong Kong. *Sustain. Cities Soc.* 31, 12–25. <https://doi.org/10.1016/j.scs.2017.01.018>.
- Lenzholzer, S., 2012. Research and design for thermal comfort in Dutch urban squares. *Resour. Conserv. Recycl.* 64, 39–48.
- Levin, N., Zhang, Q., 2017. A global analysis of factors controlling VIIRS nighttime light levels from densely populated areas. *Rem. Sens. Environ.* 190, 366–382.
- Li, F., Yan, Q.W., Bian, Z.F., et al., 2020a. A POI and LST adjusted NTL urban index for urban built-up area extraction. *Sensors* 20 (10).
- Li, L.L., Yu, T., Zhao, L.M., et al., 2019a. Characteristics and trend analysis of the relationship between land surface temperature and nighttime light intensity levels over China. *Infrared Phys. Technol.* 97, 381–390.
- Li, J.F., Wang, F.F., Fu, Y., et al., 2020b. A novel SUHI referenced estimation method for multicenters urban agglomeration using DMSP/OLS nighttime light data. *IEEE J. Sel. Top. Appl. Earth Obs. Rem. Sens.* 13, 1416–1425.
- Li, J.G., He, C.Y., Shi, P.J., et al., 2007. The use of multisource satellite and geospatial data to study the ecological effects of urbanization: a case of the urban agglomerations in bohai rim. *J. Rem. Sens.* 11 (1), 115–126.
- Li, Y.N., Song, Y.K., Cho, D., Han, Z., 2019b. Zonal classification of microclimates and their relationship with landscape design parameters in an urban park. *Landsc. Eco. Eng.* 15 (3), 265–276.
- Liu, M., Zhang, D.S., Pietzarka, U., et al., 2021. Assessing the adaptability of urban tree species to climate change impacts: a case study in Shanghai. *Urban Forest. Urban Green.* 127189 <https://doi.org/10.1016/J.UFUG.2021.127186>.
- Liu, Y.H., Fang, X.Y., Xu, Y.M., et al., 2017. Assessment of surface urban heat island across China's three main urban agglomerations. *Theor. Appl. Climatol.* 133 (1–2), 473–488.
- Luo, X., Yang, J., Sun, W., et al., 2021. Suitability of human settlements in mountainous areas from the perspective of ventilation: a case study of the main urban area of Chongqing. *J. Clean. Prod.* <https://doi.org/10.1016/j.jclepro.2021.127467>.
- Ma, T., Zhou, Y.K., Zhou, C.H., et al., 2015. Night-time light derived estimation of spatio-temporal characteristics of urbanization dynamics using DMSP/OLS satellite data. *Rem. Sens. Environ.* 158, 453–464.
- Milesi, C., Elvidge, C.D., Nemani, R.R., Running, S.W., 2003. Assessing the impact of urban land development on net primary productivity in the southeastern United States. *Rem. Sens. Environ.* 86 (3), 401–410.
- Oke, T.R., 1973. City Size and the Urban Heat Island. *Atmospheric Environment*, pp. 769–779.
- Omidvar, A., Kim, J., 2020. Modification of sweat evaporative heat loss in the PMV/PPD model to improve thermal comfort prediction in warm climates. *Build. Environ.* 176, 106868 <https://doi.org/10.1016/j.buildenv.2020.106868>.
- Ouyang, W., Morakinyo, T.E., Ren, C., Ng, E., 2020. The cooling efficiency of variable greenery coverage ratios in different urban densities: a study in a subtropical climate. *Build. Environ.* <https://doi.org/10.1016/j.buildenv.2020.106772>.
- Panagopoulos, T., Gonzalez Duque, J.A., Bostenaru Dan, M., 2015. Urban planning with respect to environmental quality and human well-being. *Environ. Pollut.* 208 (Pt A), 137–144.
- Peng, J., Hu, Y.N., Liu, Y.X., et al., 2018. A new approach for urban-rural fringe identification: integrating impervious surface area and spatial continuous wavelet transform. *Landsc. Urban Plann.* 175, 72–79.
- Peng, J., Xie, P., Liu, Y.X., Ma, J., 2016. Urban thermal environment dynamics and associated landscape pattern factors: a case study in the Beijing metropolitan region. *Rem. Sens. Environ.* 173, 145–155.
- Peng, S., Piao, S., Ciais, P., et al., 2012. Surface urban heat island across 419 global big cities. *Environ. Sci. Technol.* 46 (2), 696–703.
- Portela, C.I., Massi, K.G., Rodrigues, T., Alcántara, E., 2020. Impact of urban and industrial features on land surface temperature: evidences from satellite thermal indices. *Sustain. Cities Soc.* 56, 102100 <https://doi.org/10.1016/j.scs.2020.102100>.
- Qiao, Z., Tian, G., Xiao, L., 2013. Diurnal and seasonal impacts of urbanization on the urban thermal environment: a case study of Beijing using MODIS data. *ISPRS J. Photogrammetry Remote Sens.* 85, 93–101. <https://doi.org/10.1016/j.isprsjprs.2013.08.010>.
- Qiao, Z., Huang, N., Xu, X., et al., 2019. Spatio-temporal pattern and evolution of the urban thermal landscape in metropolitan Beijing between 2003 and 2017. *Acta Geograph. Sin.* 74, 475–489. <https://doi.org/10.11821/dlxb201903006>.
- Qin, Z.H., Zhang, M.H., Karnieli, A., et al., 2001. Mono-window algorithm for retrieving land surface temperature from landsat TM6 data. *Acta Geograph. Sin.* 68 (4), 456–466.
- Ren, C., Ng, E.Y.Y., Katschnner, L., 2011. Urban climatic map studies: a review. *Int. J. Climatol.* 31 (15), 2213–2233. <https://doi.org/10.1002/joc.2237>.
- Simona, H., Lindénb, J., David, H., et al., 2018. Modeling transpiration and leaf temperature of urban trees – a case study evaluating the microclimate model ENVI-met against measurement data. *Landsc. Urban Plann.* 174, 33–40.
- Shi, K., Yu, B., Huang, Y., et al., 2014. Evaluating the ability of NPP-VIIRS nighttime light data to estimate the gross domestic product and the electric power consumption of

- China at multiple scales: a comparison with DMSP-OLS data. *Rem. Sens.* 6 (2), 1705–1724.
- Shen, Z., Zhu, X., Cao, X., et al., 2019. Measurement of blooming effect of DMSP-OLS nighttime light data based on NPP-VIIRS data. *Spatial Sci.* <https://doi.org/10.1080/19475683.2019.1570336>.
- Song, J., Du, S., Feng, X., Guo, L., 2014. The relationships between landscape compositions and land surface temperature: quantifying their resolution sensitivity with spatial regression models. *Landsc. Urban Plann.* 123, 145–157.
- Steenefeld, G.-J., Klompaker, J.O., Groen, R.J.A., Holtslag, A.A.M., 2018. An urban climate assessment and management tool for combined heat and air quality judgements at neighbourhood scales. *Resour. Conserv. Recycl.* 132, 204–217.
- Stewart, I.D., Oke, T.R., Kravynhoff, E.S., 2014. Evaluation of the ‘local climate zone’ scheme using temperature observations and model simulations. *Int. J. Climatol.* 34 (4), 1062–1080.
- Stewart, I.D., Oke, T.R., 2012. Local climate zones for urban temperature studies. *Bull. Am. Meteorol. Soc.* 93 (12), 1879–1900.
- Sundus, S., Bassam, A.-H., 2020. The effect of building height diversity on outdoor microclimate conditions in hot climate. A case study of Dubai-UAE. *Urban Clim.* 32, 100611 <https://doi.org/10.1016/j.uclim.2020.100611>.
- Tan, J.K.N., Belcher, R.N., Tan, H.T.W., et al., 2021. The urban heat island mitigation potential of vegetation depends on local surface type and shade. *Urban For. Urban Green.* <https://doi.org/10.1016/j.ufug.2021.127128>.
- Uniform Standard for Design of Civil Buildings (GB503522019), 2019. China Architecture and Building Press, Beijing.
- Vahmani, P., Ban-Weiss, G.A., 2016. Impact of remotely sensed albedo and vegetation fraction on simulation of urban climate in WRF-urban canopy model: a case study of the urban heat island in Los Angeles. *J. Geophys. Res. Atmos.* 121 (4), 1511–1531.
- Wang, B., Cot, L.D., Adolphe, L., et al., 2017. Cross indicator analysis between wind energy potential and urban morphology. *Renew. Energy* 113, 989–1006.
- Wang, S., Ma, Q., Ding, H., Liang, H., 2016. Detection of urban expansion and land surface temperature change using multi-temporal landsat images. *Resour. Conserv. Recycl.* <https://doi.org/10.1016/j.resconrec.2016.05.011>.
- Xie, P., Yang, J., Sun, W., et al., 2022. Improved method for urban-scale ventilation analysis based on circuit theory. *Sustain. Cities Soc.* <https://doi.org/10.1016/j.scs.2022.103746>.
- Xie, P., Yang, J., Wang, H.Y., et al., 2020. A New method of simulating urban ventilation corridors using circuit theory. *Sustain. Cities Soc.* 59, 102162 <https://doi.org/10.1016/j.scs.2020.102162>.
- Xie, Y., Weng, Q., 2016. Detecting urban-scale dynamics of electricity consumption at Chinese cities using time-series DMSP-OLS (Defense Meteorological Satellite Program-Operational Linescan System) nighttime light imagery. *Energy* 100, 177–189.
- Xue, Z., Hou, G., Zhang, Z., et al., 2019. Quantifying the cooling-effects of urban and peri-urban wetlands using remote sensing data: case study of cities of Northeast China. *Landsc. Urban Plann.* 182, 92–100.
- Yang, B., Yang, X.C., Ruby Leung, L., et al., 2019. Modeling the impacts of urbanization on summer thermal comfort: the role of urban land use and anthropogenic heat. *J. Geophys. Res. Atmos.* <https://doi.org/10.1029/2018JD029829>.
- Yang, J., Luo, X., Jin, C., et al., 2020a. Spatiotemporal patterns of vegetation phenology along the urban–rural gradient in Coastal Dalian, China. *Urban Forest. Urban Green.* vol. 54, 126784 <https://doi.org/10.1016/j.ufug.2020.126784>.
- Yang, J., Jin, S.H., Xiao, X.M., et al., 2019b. Local climate zone ventilation and urban land surface temperatures: towards a performance-based and wind-sensitive planning proposal in megacities. *Sustain. Cities Soc.* 47, 101487 <https://doi.org/10.1016/j.scs.2019.101487>.
- Yang, J., Ren, J.Y., Sun, D.Q., et al., 2021a. Understanding land surface temperature impact factors based on local climate zones. *Sustain. Cities Soc.* 69 <https://doi.org/10.1016/j.scs.2021.102818>.
- Yang, J., Wang, Y.C., Xiao, X.M., et al., 2019a. Spatial differentiation of urban wind and thermal environment in different grid sizes. *Urban Clim.* 28, 100458 <https://doi.org/10.1016/j.uclim.2019.100458>.
- Yang, J., Wang, Y.C., Xiu, C.L., et al., 2020b. Optimizing local climate zones to mitigate urban heat island effect in human settlements. *J. Clean. Prod.* 275 <https://doi.org/10.1016/j.jclepro.2020.123767>, 123767.
- Yang, J., Wang, Y.C., Xue, B., Li, Y.F., Xiao, X.M., Xia, J.H., He, B.J., 2021b. Contribution of urban ventilation to the thermal environment and urban energy demand: different climate background perspectives. *Sci. Total Environ.* 795 <https://doi.org/10.1016/j.scitotenv.2021.148791>.
- Yang, J., Yang, Y.X., Sun, D.Q., Jin, C., Xiao, X.M., 2021c. Influence of urban morphological characteristics on thermal environment. *Sustain. Cities Soc.* 72 <https://doi.org/10.1016/j.scs.2021.103045>.
- Yang, X.C., Ruby Leung, L., Zhao, N., et al., 2017a. Contribution of urbanization to the increase of extreme heat events in an urban agglomeration in east China. *Geophys. Res. Lett.* 44, 6940–6950. <https://doi.org/10.1002/2017GL074084>.
- Yang, Y., Ma, M., Tan, C., et al., 2017b. Spatial recognition of the urban-rural fringe of Beijing using DMSP/OLS nighttime light data. *Rem. Sens.* 9 (11).
- Yin, S.W., Gong, Z.W., Gu, L., et al., 2022. Driving forces of the efficiency of forest carbon sequestration production: spatial panel data from the national forest inventory in China. *J. Clean. Prod.* 330, 129776 <https://doi.org/10.1016/j.jclepro.2021.129776>.
- You, H., Jin, C., Sun, W., 2020. Spatiotemporal evolution of population in Northeast China during 2012–2017: a nighttime light approach. *Complexity* 1–12. <https://doi.org/10.1155/2020/3646145>.
- Yu, C., Hu, D.Y., Zhang, Y., et al., 2019. Spatial characteristics and changes of surface thermal field in Beijing-Tianjin-Tangshan region in the last two decades. *Sci. Geogr. Sin.* 39 (6), 1016–1024.
- Yue, W.Z., Xu, L.H., 2013. Thermal environment effect of urban water landscape. *Acta Ecol. Sin.* 33, 1852–1859. <https://doi.org/10.5846/stxb201112141915>, 06.
- Yue, W.Z., Wu, T., Liu, X., et al., 2020. Developing an urban sprawl index for China's mega-cities. *J. Geogr. Sci.* 75 (12), 2730–2743. <https://doi.org/10.11821/dlxb202012013>.
- Zhao, C., 2018. Linking the local climate zones and land surface temperature to investigate the surface urban heat island, a case study of san Antonio, Texas, U.S. *ISPRS annals of photogrammetry. Rem. Sens. Spatial Inform. Sci.* IV-3, 277–283.
- Zheng, W., Zhang, Y., Xia, J., Jiang, Y., 2020. Cleaner heating in Northern China: potentials and regional balances. *Resour. Conserv. Recycl.* 160, 104897.
- Zhou, D., Bonafoni, S., Zhang, L., et al., 2018. Remote sensing of the urban heat island effect in a highly populated urban agglomeration area in East China. *Sci. Total Environ.* 628–629, 415–429.
- Zhou, D., Li, D., Sun, G., et al., 2016. Contrasting effects of urbanization and agriculture on surface temperature in eastern China. *J. Geophys. Res. Atmos.* 121 (16), 9597–9606.
- Zhou, Y., Ma, T., Zhou, C., et al., 2015. Nighttime light derived assessment of regional inequality of socioeconomic development in China. *Rem. Sens.* 7, 1242–1262.